Quasi-One-Dimensional Magnons in an Intermetallic Marcasite

M. B. Stone, M. D. Lumsden, S. E. Nagler, D. J. Singh, J. He, B. C. Sales, and D. Mandrus

Quasi-one-dimensional magnons in an intermetallic marcasite

M. B. Stone,[1] M. D. Lumsden,[1] S. E. Nagler,[1] D. J. Singh,[2] J. He,[3] B. C. Sales,[2] and D. Mandrus[2, 4]

[1]*Neutron Sciences Directorate, Quantum Condensed Matter Division,*
Oak Ridge National Laboratory, Oak Ridge, Tennessee 37831, USA
[2]*Materials Science and Technology Division, Oak Ridge National Laboratory, Oak Ridge, Tennessee 37831, USA*
[3]*Department of Physics and Astronomy, Clemson University, Clemson, SC 29634, USA*
[4]*Department of Materials Science and Engineering,*
University of Tennessee, Knoxville, Tennessee 37996, USA

We present inelastic neutron scattering measurements and first principles calculations examining the intermetallic marcasite $CrSb_2$. The observed spin wave dispersion implies that the magnetic interactions are strongly one-dimensional with antiferromagnetic chains parallel to the crystalline c-axis. Such low-dimensional excitations are unexpected in a semiconducting intermetallic system. Moreover we observe a clear anisotropic thermal conductivity indicating that the magnetic anisotropy enhances thermoelectric properties along particular crystallographic directions.

Efficient and cost-effective power generation has revived interest in thermoelectric materials in an energy resource dominated economy. $CrSb_2$ has gained recent attention as a narrow gap semiconductor with potential thermoelectric properties. Investigations into substitutional compounds such as $CrSb_{2-x}Te_x$ [1, 2], $CrSb_{2-x}Sn_x$[2] and $Cr_{1-x}Ru_xSb_2$ [3] have found changes in the electronic properties, with an increase in the thermoelectric figure of merit for Te substitution. $CrSb_2$ has also been considered as an electrode material for lithium based batteries showing improvement compared to using pure antimony.[4, 5] Here we report inelastic neutron scattering (INS) measurements and first principles calculations for this compound. We find that $CrSb_2$ has significant exchange anisotropy exhibiting a quasi-one-dimensional (1d) magnon spectrum. The determined exchange constants and anisotropy allow one to classify $CrSb_2$ as an $S = 1$ antiferromagnetic (AFM) chain with interchain coupling and on-site anisotropy. We find that the anisotropic magnon spectrum results in an anisotropic thermal conductivity over a broad temperature range. Low-dimensional excitations are unexpected in a semiconducting intermetallic system, and our observations are the first spectroscopic evidence of quasi-one-dimensional antiferromagnetic exchange in such a material.

$CrSb_2$ is an intermetallic marcasite where the Cr atoms are located at the body center and corner positions of the orthorhombic unit cell with room temperature lattice constants $a = 6.028$, $b = 6.874$, and $c = 3.272$ Å.[6] The Cr atoms are at the center of a distorted octahedron of Sb sites as shown in Fig. 1. Early thermodynamic measurements found $CrSb_2$ to have AFM correlations[8, 9], but the ordered magnetic phase with $T_N = 273(2)$ K was not observed until much later.[7] The ordered magnetic structure is shown in Fig. 1 where the moments are roughly perpendicular to the (101) plane. This magnetic structure results in magnetic Bragg peaks

at the $(H \; \frac{2K+1}{2} \; \frac{2L+1}{2})$ positions where H, K, and L are the Miller indices of the chemical unit cell. The body centered Cr sites form the identical AFM structure as the corner sites, albeit displaced along the [111] direction. The magnetic unit cell is doubled along the b and c axes with an ordered moment corresponding to spin $S = 0.97(2)$ as determined from neutron diffraction measurements.[7] Early band structure considerations have shown that there are two localized d electrons per Cr^{4+} in $CrSb_2$. [10]

Local spin density approximation (LSDA) calculations were performed using the general potential linearized augmented planewave (LAPW) method.[11] Local orbital extensions were employed to include the high lying semicore states and to relax any linearization errors. The calculations included no shape approximations to either the potential or charge density. Relativity was included for the valence states within a scalar relativistic approximation, while full relativity was included for the core states,
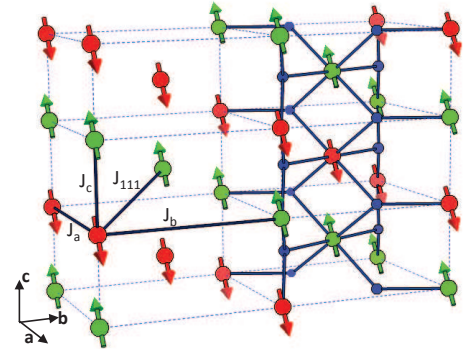

FIG. 1: (color online)Nuclear and magnetic structure of $CrSb_2$.[6, 7] Red and green spheres are Cr sites, where the vector and color represent the spin orientation. Small blue spheres are the Sb sites shown only for the three unit cells on the right of the figure for clarity. Nearest neighbor exchange constants are labeled and shown as heavy black lines.

within an atomic like approximation. Well converged basis sets consisting of more than 850 LAPW functions plus local orbitals were used for the primitive unit cell (two formula units) of $CrSb_2$. Brillouin zone samplings were done with the special **k**-points method, using 128 **k**-points in the irreducible wedge of the primitive cell and equivalent samplings for the larger AFM cells.

We consider ferromagnetic (FM) and several AFM ground states including the ordered magnetic structure found for $CrSb_2$, which we denote as AFM-D. Other AFM structures include doubled magnetic cells along the a (AFM-A) and b (AFM-B) axes, and FM correlations within each of the sublattices but AFM relative to one another (AFM-G). The lowest calculated LSDA energy is found for AFM-D, -0.522 eV per formula unit relative to the non-spin polarized case, with other values listed in Fig. 2. All of the configurations were found to be conducting except for AFM-D. The calculated density of states for AFM-D is shown in Fig. 2. The calculated bandgap of 0.07 eV agrees with low temperature resistivity measurements. [12] The large energy difference between the AFM-D and FM structures compared to the relatively low T_N in a lattice with no geometrical frustration suggests interesting magnetic correlations. The energy of the AFM-G state is 0.025 eV per Cr higher than the FM state, indicating that the inter-sublattice coupling, J_{111} in Fig. 1, is very weak and likely FM. The energy of the other AFM states implies weak FM exchange along a, almost no interaction along b, and strong AFM exchange along c in agreement with the ordered magnetic structure. The large AFM exchange along the c axis would make the magnetic correlations in $CrSb_2$ quasi-1d, thus explaining the suppressed value of T_N.[13] This also explains the difficulty in observing the phase transition in prior thermodynamic measurements. The 1d magnetism would result in much of the magnetic en-
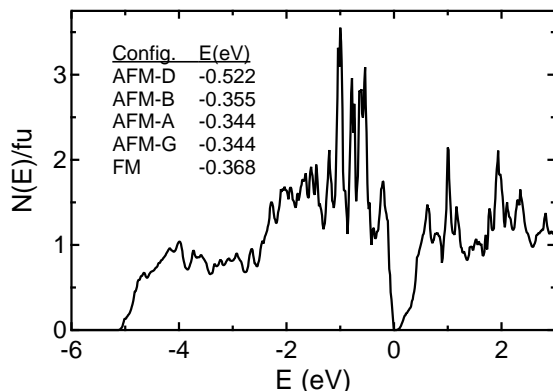

FIG. 2: LSDA calculated electronic density of states $N(E)$ per formula unit (fu) for the AFM order of the magnetic ground state (AFM-D). The table inset lists the configurations and calculated LSDA energies per formula unit relative to the non-spin-polarized case (see text).

tropy being exhausted with a very broad hump in susceptibility as the local order develops, with only smaller features at T_N.

Single crystal INS provides an efficient probe of the LSDA predictions of the exchange coupling for $CrSb_2$. Single crystals were grown from an Sb flux with a starting composition of $CrSb_{16}$. The material was heated in vacuum in a 10 cc alumina crucible to 1273 K, held for 24 h, and then cooled to 913 K at 1 K/hr. The excess Sb liquid was centrifuged away, leaving crystals with typical dimensions of 5x5x5 mm^3. Single crystal INS measurements of $CrSb_2$ were performed at the HB3 triple-axis spectrometer (TAS) and the ARCS chopper spectrometer at Oak Ridge National Laboratory's High Flux Isotope Reactor and Spallation Neutron Source respectively.[14] Measurements at HB3 were performed for samples in the (0 K L)[$m \approx 4.05$ g] and (H L L)[$m \approx 3.5$ g] scattering planes. The instrument was configured with a vertically focused Be (002) monocrhomator and a PG (002) analyzer with fixed final energy $E_f = 30.5$. Pyrolytic graphite filters were in place between the sample and analyzer. Constant wave vector, **Q**, and energy transfer, $\hbar\omega$, scans were performed primarily along the (H $\kappa/2$ $\kappa/2$), (0 K $\kappa/2$) and (0 $\kappa/2$ L) directions, where $\kappa = 1$ or 3 between 5 and 70 meV. Data were acquired for a fixed monitor count unit (mcu) to account for variations in neutron flux as a function of incident energy, E_i. Measurements at ARCS were performed with the (0 K L) plane in the equatorial plane of the instrument with $E_i = 150$ meV neutrons. Data were measured by rotating about the vertical (1 0 0) axis in increments of 0.75 degrees over a total of 62 degrees with the incident wave vector initially pointed 9 degrees from the (0 1 0) direction. Data were normalized to the accumulated charge on the source and histogramed into **Q** and $\hbar\omega$ space.

Figure 3 shows the measured scattering intensity as a function of $\hbar\omega$ and **Q** for $CrSb_2$ at $T = 10$ K. Given the inversion symmetry of the magnetic structure, the data from ARCS, Fig. 3(d)-(f), have been averaged for data acquired at $\pm$**Q** and for higher **Q** Brillouin zones scaled by the Cr magnetic form factor. Data have been background subtracted using data scaled from larger Brillouin zones to suppress phonon scattering. There is a clear single excitation that disperses along all three principal axes. The overall minimum in the dispersion appears at ≈ 25 meV at $(H, \frac{2K+1}{2}, \frac{2L+1}{2})$ for integer H,K and L. The kinematic limits of the TAS measurements did not allow us to follow this mode above 60 meV for small values of |**Q**|. The ARCS measurements are able to observe this mode up to its maximum energy of ≈ 78 meV. The bandwidth along the H and K direction is 13.3 and 14.8 meV respectively, and the bandwidth of the excitation along L is 53.6 meV.

The scattering intensity falls off rapidly with |**Q**| indicating magnetic fluctuations, and the greatest dispersion is along the c-axis. Prior investigations of the high tem-
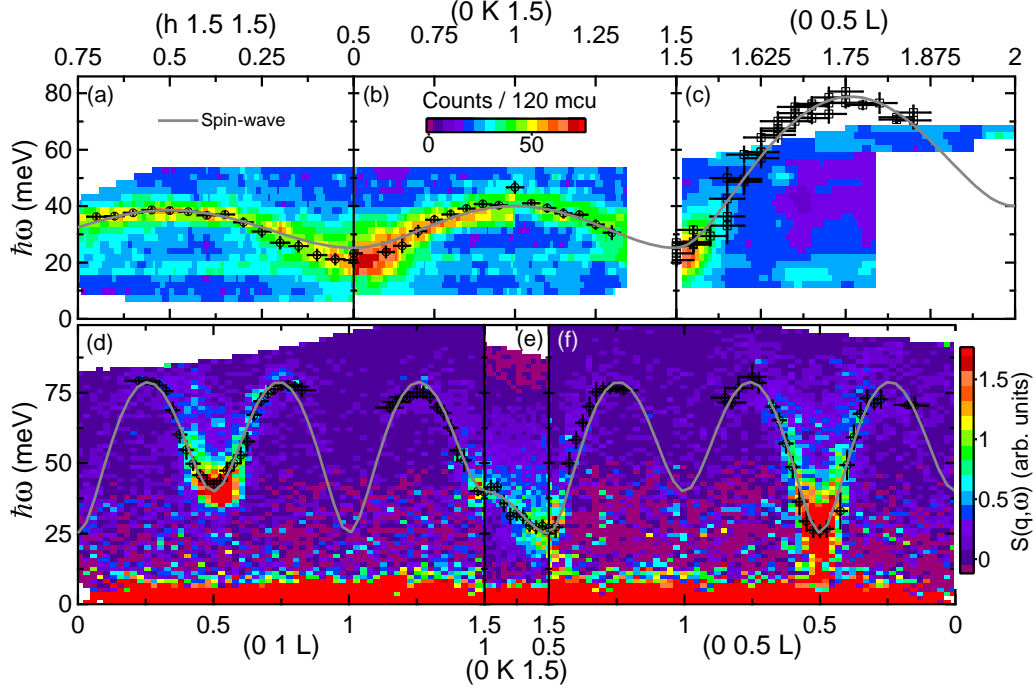
FIG. 3: (Color online) $T = 10$ K INS spectra of CrSb$_2$ along principal axes of the reciprocal lattice. (a)-(c)[(d)-(f)] Data were measured using HB3[ARCS]. (d)-(f) Have been background subtracted as described in the text. (a)[(b)-(f)] were measured with the sample in the (H K K)[(0 K L)] scattering plane. Open circles correspond to peak positions determined from extracted constant $\mathbf{Q}$ scans as described in the text. Open squares in (c) correspond to peak positions from ARCS and HB3 constant $\mathbf{Q}$ scans along the $(H \frac{(2K+1)}{2} L)$ directions where H and K are integers. Vertical[Horizontal] error bars represent the fitted peaks full width at half maximum [range of $\mathbf{Q}$ integration]. The grey solid line is the fitted spin-wave dispersion described in the text.

perature magnetic susceptibility employed a two-state magnetic system with an energy gap of 70.7 meV to describe the results.[12] Although this value is within the energy scale of the measured magnon, it is quite far from the peak in the magnetic density of states. Our INS measurements provide a picture of the microscopic interactions in this material, and clearly shows that the gap in the magnetic spectrum is approximately 25 meV.

We project the data from ARCS and HB3 into a collection of constant $\mathbf{Q}$ scans by integrating over ± 0.05 rlu in each of the principal axes directions. These individual scans are then fit to a single inelastic Gaussian peak for $20 < \hbar\omega < 80$ meV, allowing us to extract the dispersion of the magnetic excitation. A portion of these fitted peak positions is shown in Fig. 3. The points in Fig. 3(c) are from a series of $\mathbf{Q}$'s along the $(\eta \frac{2\kappa+1}{2} L)$ direction where η and κ are integer values measured with both HB3 and ARCS. This panel illustrates the extent of the dispersion along the L direction. Although the electronic band-gap is small, we consider the cooperative magnetism in CrSb$_2$ to be local moment in nature. This allows one to use linear spin wave theory (LSWT) to calculate a dispersion relation, $\hbar\omega(\mathbf{Q})_{SW}$ for comparison to the measured data. The tilts and distortion of the Cr-Sb octahedron, the direction of the ordered moments, and the gap in the AFM

spectrum implies the need for an anisotropy parameter, D. The Heisenberg Hamiltonian then becomes

$$\mathcal{H} = \sum_{\alpha} \sum_{\langle ij \rangle_\alpha} J_\alpha \mathbf{S}_i \cdot \mathbf{S}_j + \sum_i D(S_z^2)_i, \qquad (1)$$

where α is summed over a, b, and c, and we define the z axis to be along the ordered moment.[15, 16] This results in the spin-wave dispersion

$$A_{\mathbf{Q}} = 2S[J_a[\cos(2\pi H) - 1] + J_b + J_c + D]$$
$$B_{\mathbf{Q}} = 2S[J_b \cos(2\pi K) + J_c \cos(2\pi L)]$$
$$\hbar\omega(\mathbf{Q})_{SW} = \sqrt{A_{\mathbf{Q}}^2 - B_{\mathbf{Q}}^2}, \qquad (2)$$

where S is the magnitude of the spin quantum and the exchange interactions are illustrated in Fig. 1. Fitting to $\hbar\omega(\mathbf{Q})_{SW}$ with $S = 1$ results in the solid grey line in Fig. 3 and the parameters $J_c = 35.7(2)$, $J_a = -1.31(6)$, $J_b = 1.69(7)$ and $D = 2.07(9)$ meV. Including a J_{111} exchange constant has negligible improvement on the χ^2 of the fit. LSWT accounts well for the measured low-temperature dispersion in CrSb$_2$. The resulting values also agree well with the FM and AFM spin-spin interactions based upon the low temperature ordered magnetic structure, and the predictions based upon LSDA calculations discussed earlier. The J_c exchange is an order of
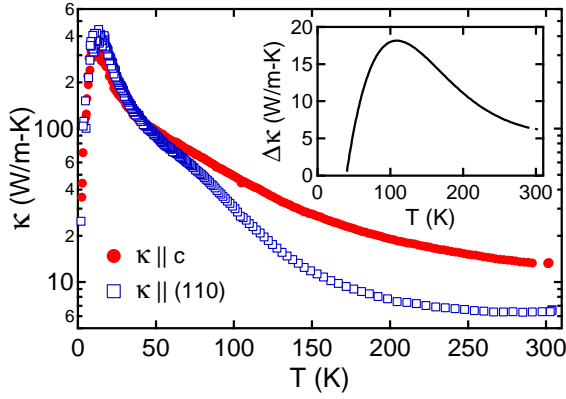
FIG. 4: (color online)Thermal conductivity of $CrSb_2$ as a function of temperature. Main panel illustrates thermal conductivity as measured along orthogonal crystallographic directions. Inset is the difference of the data in the main panel $(\kappa(c) - \kappa(110))$ for $T > 50$ K as described in the text.

magnitude larger than along the other axes in support of the predicted quasi-1d magnon behavior.

For $T > T_N$, the magnetic excitations in $CrSb_2$ could be considered $S = 1$ quasi-1d magnons propagating out of a spin-liquid ground state suggesting comparison to a Haldane chain dispersion. Thermal population of phonons makes an accurate comparison using INS difficult at high temperatures, but the extracted exchange constants based upon LSWT for $T < T_N$ place $CrSb_2$ well within an ordered phase of the phase diagram.[17, 18] Measurements of the narrow-gap semiconducting marcasite $FeSb_2$ have found this system to be nearly magnetic, and that substitution with Cr as $Fe_{1-x}Cr_xSb_2$ with $x \geq 0.45$ pushes the system into the AFM phase with T_N increasing with x.[19, 20] Although INS of $FeSb_2$ observed no clear magnetic excitations,[21] investigations into suppressing the T_N of $CrSb_2$ via chemical substitution are fundamentally interesting to try to move through the Haldane phase diagram and ultimately access the spin-liquid Haldane phase. Another route to adjusting the exchange constants along with the electrical conductivity would be to change the atomic percent of Sb. The high temperature trend of the magnetic susceptibility is very similar for the range of compositions between $CrSb_{1.75}$ to $CrSb_5$.[9]

The quasi-1d magnetic excitation spectrum of $CrSb_2$ will affect its thermoelectric properties. Thermal transport measurements have been performed for other low-d magnets. In the case of the $S = \frac{1}{2}$ spin-ladder $Sr_{14-x}Ca_xCu_{24}O_41$[22, 23] and the $S = 1$ Haldane chain NENP[24], it was found that thermal transport was enhanced along the 1d axis by a factor of up to ≈ 15. We performed thermal conductivity measurements between 5 and 300 K using a commercial apparatus with single crystals with typical dimensions of $8X1.5X1.5$ mm^3. Trans-

port was measured parallel and perpendicular to the c-axis. The perpendicular measurements were made along the (110) axis. The error in these measurements is approximately $\pm 10\%$ and is due primarily to errors in the measurement of crystal dimensions. Figure 4 shows these measurements, and above $T \approx 50$ K there is enhanced thermal transport along the c-axis which is consistent with our expectation based upon the magnetic spectrum. The inset of Fig. 4 is the difference between the two measurements and indicates an enhanced thermal conductivity along the 1d axis for a range of temperatures up to and beyond T_N. The results shown in Fig. 4 are consistent with the picture of a nearly isotropic lattice conductivity above the low-temperature peak combined with a thermally activated c-axis magnetic contribution that becomes significant for $T > 50$ K. The electrical resistivity in the two directions is different, and this difference has been accounted for in the inset using the Wiedemann-Franz law. This has a very minor effect on the data, since the resistivity of $CrSb_2$ is relatively high. This correction has no effect on the thermal conductivity data below 200 K. These measurements indicate that the thermoelectric figure of merit may be improved by orienting the 1d axis orthogonal to the flow of charge. While the lattice thermal conductivity is likely dominant, the magnetic contribution is important and it along with its anisotropy should be considered when assessing the thermoelectric properties of $CrSb_2$.

[1] H. J. Li *et al.*, Mat. Sci. Eng. B **149**, 53 (2008).
[2] H. Li *et al.*, Chi. J. Mat. Res. **24**, 429 (2010).
[3] Y. Takahashi *et al.*, J. Alloys Compds. **459**, 78 (2008).
[4] F. J. Fernández-Madrigal *et al.*, J. Electro. Chem. **501**, 205 (2001).
[5] C-M. Park and H. J. Sohn, Electrochimica Acta, **55**, 4987 (2010).
[6] H. Holseth and A. Kjekshus, Acta Chem. Scand., **22**, 3283 (1968).
[7] H. Holseth, *et al.*, Acta Chem. Scand., **24**, 3309 (1970).
[8] G. Foëx and M. Graff, Compt. rend. **209**, 160 (1939).
[9] H. Haraldsen, *et al.*, Arch. Math. Naturvidenskab, **50**, No. 4., 95-135 (1948).
[10] J. B. Goodenough, J. Solid State Chem., **5**, 144 (1972).
[11] D. J. Singh, *Planewaves, Pseudopotentials and the*

LAPW method, Kluwer Academic, Boston (1994).

[12] K. Adachi, *et al.*, J. Phys. Soc. Jpn. **26**, 906 (1969).

[13] D. J. Scalapino, *et al.*, Phys. Rev. B **11**, 2042 (1975).

[14] D. L. Abernathy, *et al.*, Review of Sci. Inst. (in press), (2012).

[15] S. W. Lovesey, *Theory of Neutron Scattering from Condensed Matter: Volume 2* (Clarendon Press, Oxford, UK 1987).

[16] P. A. Lindgård, *et. al*, J. Phys. Chem. Solids **28**, 1357 (1967).

[17] T. Sakai and M. Takahashi, Phys. Rev. B **42** 4537 (1990).

[18] A. Zheludev, *et al.*, Phys. Rev. B **62**, 8921 (2000).

[19] C. Petrovic, *et al.*, Phys. Rev. B **67**, 155205 (2003).

[20] R. Hu, *et al.*, Phys. Rev. B **76**, 115105 (2007).

[21] I .A. Zaliznyak, *et al.*, Phys. Rev. B **83**, 184414 (2011).

[22] A. V. Sologubenko, *et al.*, Phys. Rev. Lett. **84**, 2714 (2000).

[23] C. Hess, *et al.*, Phys. Rev. B **64**, 184305 (2001).

[24] A. V. Sologubenko, *et al.*, Phys. Rev. Lett. **100**, 137202 (2008).